May 16th, 3:15 PM

Modeling of Tide Gate to Improve Fish Passability

L. Cassan
IMFT, Université de Toulouse, CNRS, lcassan@imft.fr

Léo Guiot
IMFT, Université de Toulouse, CNRS, lguiotde@imft.fr

Gilles Belaud
UMR G-EAU, belaud@supagro.fr

Recommended Citation

Cassan, L. (2018). Modeling of Tide Gate to Improve Fish Passability. Daniel Bung, Blake Tullis, 7th IAHR International Symposium on Hydraulic Structures, Aachen, Germany, 15-18 May. doi: 10.15142/T3BW72 (978-0-692-13277-7).

7th International Symposium on Hydraulic Structures Aachen, Germany, 15-18 May 2018
ISBN 978-0-692-13277-7 DOI: 10.15142/T3BW72

Modeling of Tide Gate to Improve Fish Passability

L. Cassan[1], L. Guiot[1] & G. Belaud[2]
[1]*Institut de Mécanique des Fluides de Toulouse, IMFT, Université de Toulouse, CNRS - Toulouse, FRANCE*
[2]*UMR-GEAU, Montpellier, France*
E-mail: lcassan@imft.fr

Abstract: *Tidal gates are hydraulic structures that prevent salt water from entering in freshwater marshes. However, they also block fish migration. For a side hinged gate, the migration can be facilitated by maintaining a little opening during all the tide. In this paper, the discharge coefficient of such a gate is evaluated based on numerical and experimental studies. It is found that the experimental discharge coefficients evolve with the difference between upstream and downstream water depths. Using shallow water simulations to estimate energy loss, we derived a model able to predict discharge with reasonable accuracy. An output of the model is the design of a stiffener device that limits salt water intrusion at high tide. Resolving the angular momentum, the optimal stiffener stiffness can be found to maintain opening sufficient for migration, while reducing greatly the volume of salt water intrusion in comparison with a constant block.*

Keywords: *Tide Gate model, tide gate management, gate design, fish passage, water quality.*

1. Introduction

Tide gates are common structures in coastal areas. Their objective is to control water and salt exchange between marshes and sea. They have a major impact on water flows in rivers and can impact water surface profiles up to several kilometers upstream. Most of the time, they are fully open or fully closed. In order to design improved management strategies, aiming at improving flood prevention, fish connectivity (Boys et al. 2012, Wright et al, 2014), or pollution management, it is essential to use accurate models for stage-discharge-opening relationships. The studied structure is a common gate in the French coastal marshes. It consists of a side-hinged rectangular tide gate rotating around a vertical axis. It closes when the sea level is above the marsh level and opens otherwise. A new soft design improvement is proposed, consisting of blocks and/or stiffeners. In particular, the stiffener would introduce a delay between flow inversion and gate closure, giving enough time to catadromous/anadromous fishes to penetrate in the hydrographic network at the tide beginning (Lauronce et al. 2015). Near the maximum tidal level, the gate would be closed to avoid seawater inflow causing bank erosion, suspended material and salt intrusion. The stiffener could be associated to a shim to let the gate open during all tide, with a maximum opening at the tide beginning. This management could be adapted to European Eel migration for which it is observed that they come in during tide with a preference for tide beginning (1 or 2 hours before high tide).

Figure 1. block on a side-hinged gate (left) and stiffener on a Top-hinged gate (right) (Lauronce et al. 2015)

In this paper, we propose to evaluate the design of a stiffener aiming at improving fish migration without excessive seawater intrusion during high tides. To do so, we needed to derive a discharge coefficient model of this structure. A theoretical model was developed based on energy balance, and calibration with a 2D shallow water. The derived model was checked thanks to experiments on a 1:10 scale model. Finally, design relationships are proposed considering several stiffener implementations.

2. Discharge Analytical modeling

2.1. Flow configurations

The flow passes through the tide gate from the sea (upstream) to the marsh (downstream). To enable the passability, the gate is maintained open at a given angle (θ). In practice, this opening is obtained with a block or a stiffener that prevents the leaf from closing totally. The size of the block can be chosen according to the saltwater volume that can be accepted in the marsh. The upstream water depth is denoted $h_u$and the downstream water depth h_d.

Near the opening, a plunging jet appears causing the velocity to reach a maximum (denoted Vj) at a contracted section where the water depth reaches the depth h_d. The width of the contracted section w_j defines the lateral contraction coefficient $C_c = w_j/w$. The non-uniformity of the velocity distribution will be taken into account in the kinetic energy term with the Coriolis coefficient α at the contracted section.

The gate opening *w* depends on the gate configuration. It is defined by 2 different lengths as a function of the ratio between the channel width (*B*) and the gate leaf width *(l*). Indeed if the gate is too wide, the channel sidewall constrains the flow, and influences the jet through the gate.

When a wall or a totally closed gate leaf is encountered on one side, the flow is deviated to the opposite sidewall. Here we consider the case of *B/l*=2 which corresponds to a tide gate composed by two gate leaves of same size.

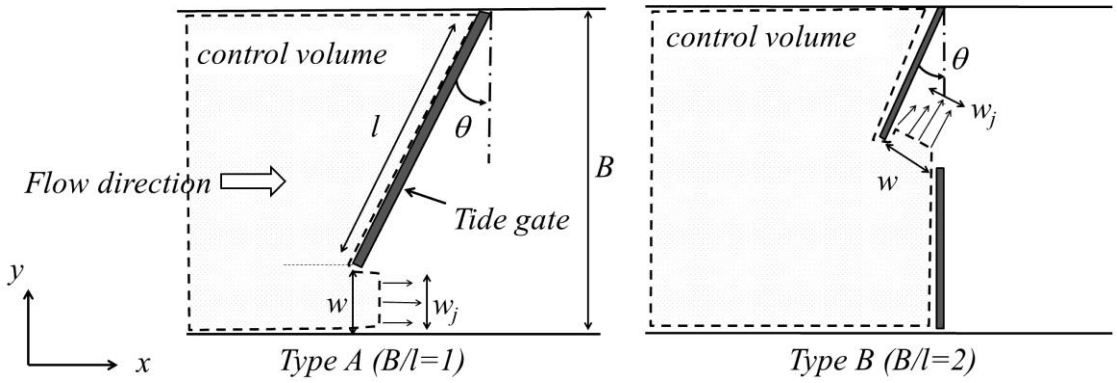

Figure 2. Characteristic lengths and flow configuration as a function of B/l

To obtain a unified formula for the discharge coefficient (C_d) the opening is obtained by calculating the distance between the gate and the fixed side or leaf:

$$w = \min\left(B - l\cos\theta, l\sqrt{2(1-\cos\theta)}\right) \quad (1)$$

The discharge coefficient is defined with the upstream water depth (h_u) applied to the whole control volume and the downstream water depth (h_d). We considered a constant depth for each control volume (delimited by dotted lines in Fig. 2). The total flow rate is denoted by $Q$and deduced from study of vertical slot fishway (Wang et al. 2010).

$$Q = C_d w h_u \sqrt{2g(h_u - h_d)} \quad (2)$$

2.2. Energy balance

The energy balance in the upstream control volume (Fig. 2) gives the first relationship between C_d and the hydraulic conditions. It is assumed that no head loss occurs in this volume because velocity magnitude and gradients are low. The subscripts *u*, *d* refer respectively to the upstream section and downstream section.

$$h_u + \alpha_u \frac{1}{2g}\left(\frac{Q}{Bh_u}\right)^2 = h_d + \alpha_d \frac{1}{2g}\left(\frac{Q}{w_j h_d}\right)^2 \quad (3)$$

Where α_u and $\alpha_d$are the Coriolis coefficients upstream of the gate. In the following, we assumed that α_u=1. In dimensionless form, equation 3 becomes:

$$1 - X = \frac{1}{2}F_0^2\left(\frac{\alpha_d}{(aC_cX)^2} - 1\right) \quad (4)$$

With ${F_0}^2 = Q^2/(gB^2h_u^3)$ Froude number, $X = h_d/h_u$ (water depth ratio) and $a = w/B$ (relative opening).

Moreover Eq. (2) gives:

$$C_d = \frac{F_0}{a}\frac{1}{\sqrt{2(1-X)}} \quad (5)$$

Combining Eqs. (4) and (5), it is possible to compute the discharge coefficient for a given flowrate and water depth ratio *X*. The value of α_d and C_c will be obtained thanks to the shallow water simulation.

$$C_d = C_c\sqrt{\frac{1-X}{\frac{\alpha_d}{X^2}-(aC_c)^2}} \quad (6)$$

Where *a* is a function of the opening angle (Eq. 1).

3. Discharge model calibration

3.1. Experimental device

Experiments were conducted in a 1:10 scaled model at the IMFT laboratory. The channel is 4 m long, 0.4 m wide with glass wall. A vertical weir allows maintaining a given water depth at the downstream end. The flow rate is measured with an electromagnetic flowmeter. The tide gate consists of a PVC flat plate of 10 mm of thickness that can turn around a vertical axis. For type B, a second flat plate is set at the opposite channel side.

The angle between the gate and the cross section is denoted θ. The angle values tested are 10, 20 and 30 degrees in order to cover a reasonable opening range to allow glass eels passing.

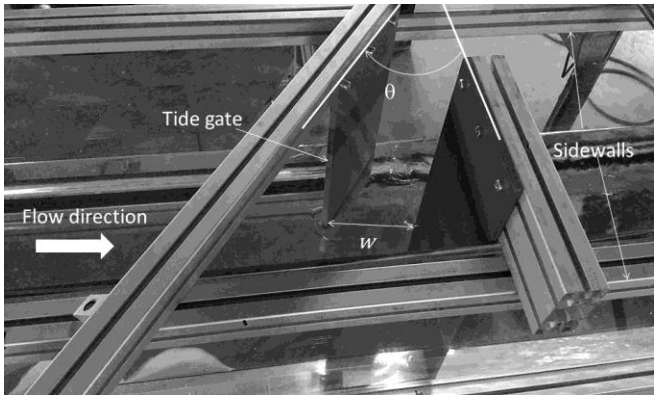

Figure 3. Top view of the experimental device.

3.2. Shallow water modeling

A shallow water model of the 2 flow types was used to provide macroscopic parameters such as Coriolis coefficients and dissipation rate. These parameters will be used further for the energy balance through the gate. Numerical methods are used to better understand the flow properties (turbulence, gradient) which could be important for fish passing. Compared to experimental correlation, they allow increasing accuracy of the discharge coefficient because they validate the analytical model (see further) for a larger range of hydraulic configurations.

The 2D shallow water model (Telemac2D) resolved the shallow water equation with a k-ε model which is adequate to compute flow for hydraulic structure where the turbulent viscosity is not constant (Tran et al. 2015). A finite element method is used for the numerical scheme, the time step is 1 ms and the total simulation time is 100 s. The computational domain corresponds to the experiments described below. The channel is 4 m long, 0.4 m wide with no bed slope.

The mesh size is 2 mm near the gate and around 1 cm otherwise. A mesh convergence study proved that this mesh size was sufficient to obtain a non-mesh dependent solution.

The boundary conditions are a constant flow rate at the upstream end and a fixed water depth at the downstream end. Manning coefficient of all walls was set to 0.0125. The simulations were carried out for 5 different flowrates (1, 3, 5, 10, 15 l/s), 3 opening angle (10, 20, 30 degree) and for type A and B. The tail water depths are 10, 15, 20 and 25 cm.

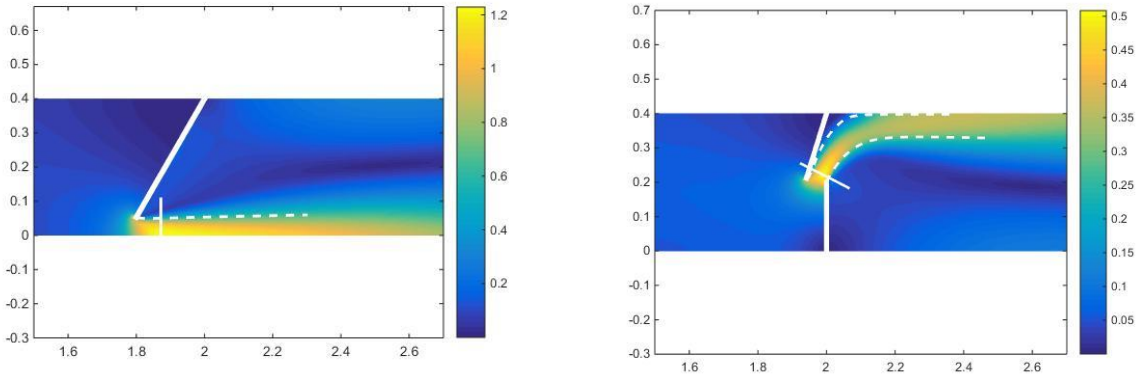

Figure 4. Velocity field, side streamline (dashed line) and contracted section (solid line) : B/l=1, Q=10 l/s, h_d=20 cm (left), B/l=2, Q=5 l/s, h_d=20 cm (right). The colorbar gives the velocity magnitude (m/s).

Firstly, the shallow water simulations give an overview of the flow as a function of the type, opening and discharge. Figure 4 shows the velocity fields downstream of the gate. For type A, the flow remains close to the sidewall. On a transverse section, the maximum velocity is at the sidewall because slip condition is used in the model. The total maximum velocity is obtained in a section with the shallowest water depth which is not necessarily where lateral contraction is at its maximum.

For type B, the flow is oriented in the gate leaf direction, then it is deflected by the sidewall until the downstream end. The contraction is larger than for type A, and a zone with very low velocity is present close to the downstream gate leaf. At the contracted section, the flow is not perfectly normal to the opening direction but it is slightly deviated in the longitudinal direction. This behavior is clearer when $\theta = 20°$. For full opening, the flow is in the longitudinal direction. The contracted cross section is defined as the section where the velocity is maximum.

The Coriolis coefficients α are obtained by the integration of u^3 at the contracted section. Although the velocity profiles show that the lateral diffusion is quite high in the total cross section, the α values are close to 1 (figure 5) because it is computed only for the contracted section. A constant value of 1.08 is considered for the following calculation. Figure 6 indicates that the contraction coefficient is almost 1 for type A because the flow is expanding in the lateral direction when the vertical contraction (and maximum velocity) is reached. But for type B, the contraction coefficient is lower and it is crucial to take its variation into account in the energy balance by considering a limited range of angle. The contraction coefficient varies little with the water depth ratio X, but it depends on the opening angle. In the

following, it is assumed a linear variation if w/h_u < 0.25 and C_c =0.75 otherwise. An analytical estimation of C_c could be deduced from an EMB method (Belaud et al., 2009), but this is out of the scope of this paper.

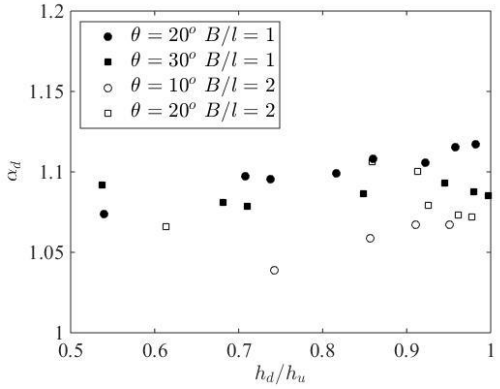

Figure 4. Coriolis coefficient at the contracted section.

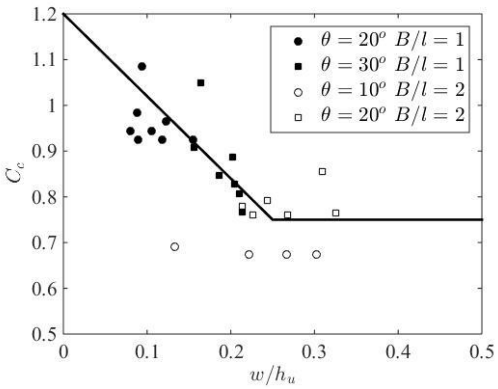

Figure 5. contraction coefficient.

3.3. Discharge coefficient

Discharge coefficients obtained by shallow water model and experiments are shown in figure 8 for *B/l*=1 and figure 9 for *B/l*=2. The C_d from energy balance is calculated with the minimum and maximum values of B/h_u, for which C_c is between 0.75 and 1 (Figure 6). The ratio B/h_u has to be considered because the experimental correlation of Cc depends on w/h_u, (w/B is fixed by the opening) for the C_d computation. Different ratios B/h_u lead to significant evolution of C_d as shown in figure 7. The difference between energy balance and shallow water calculation is mainly due to parameter α and C_c assumed to be constant. As the parameters are extracted from the simulation, the results have to be identical in order to verify the energy balance for the shallow water simulation.

For *B/l*=1, the experimental results differ significantly from shallow water simulation. It seems that flow rate is higher in experiments than in calculation. The difference is larger for small opening where the discharge is relatively low, while the head losses have the same order of magnitude than head difference. It also possible that the simulation overestimates the dissipation near stagnation points, which is a well-known disadvantage of k-ε model (Cassan et al. 2012). Moreover, small opening and small X correspond to large Froude number in the jet, and Tran et al. (2015) have shown that shallow water is not totally pertinent in these conditions.

For *B/l*=2, the ratio B/h_u has no influence since C_c is assumed to be constant for θ>10°. The experimental C_d are higher than the computed ones (figure 8). This gap can also be due to neglected head losses and underestimation of the computed dissipation.

For the next part of the study, it is important to notice that the variation of C_d can reach 30% when h_d/h_u varies, so this variation needs to be taken into account. Secondly, for B/*l*=2, the energy balance with C_c=0.75 provides a good estimation of the discharge coefficient. As the case *B/l*=2 represents a tide gate not influenced by sidewall, it is the most encountered in practice and it will be considered in the following.

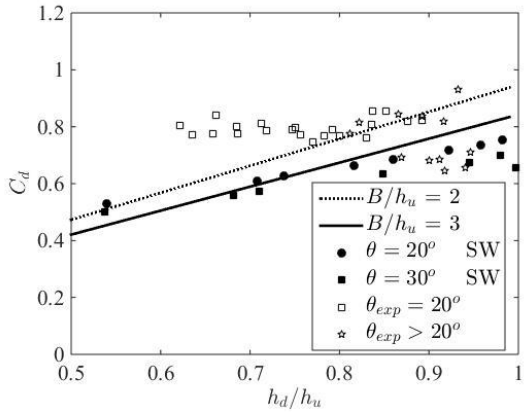

Figure 6. Discharge coefficients for *B/l*=1 model with θ=20°.

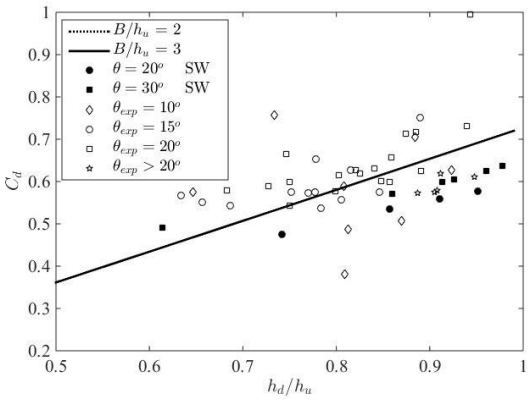

Figure 7. Discharge coefficient for *B/l*=2 model with θ=20°

4. Stiffener design and application

The opening angle θ varies with time, depending on the water levels in the upstream and downstream pools that exert a pressure on the gate. Therefore, the angular momentum balance is applied to the gate leaf with an inertial moment at rotational axis (A) denoted J_A (figure 9). The pressure forces on the upstream side of the gate (F_{gu}) and on the downstream side (F_{gd}) are assumed to be hydrostatic *i.e.* the tangential and vertical velocities are neglected. As the force is constant in the transverse direction, the application point is located at *l*/2. A stiffener is used to apply a force (*Fs*) in the x direction. The unloaded length of the stiffener is $l_0 = l_r \cos\theta_*$, and when the gate just touches the stiffener the opening angle is then θ_*.

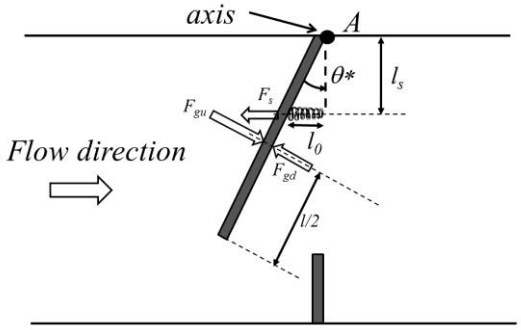

Figure 8. Stiffener device for a side-hinged tide gate.

Applying the angular momentum balance at A around the vertical axis passing through A it yields:

$$\left(F_{gu} - F_{gd} - F_a\right)\frac{l}{2} \quad - F_s \cos\theta \, l_r = \frac{d(J_A\dot{\theta})}{dt} \tag{7}$$

Where F_a is the force exerted by the air on the downstream gate on the area $l(h_u - h_d)$. For the rest of the gate, the force exerted by the air is equal on the both side of the leaf. Introducing the hydrostatic pressure, the angular momentum is:

$$\frac{1}{2}\rho g\left(h_u^2 - h_d^2\right)\frac{l^2}{2} \quad + k(\tan\theta - \tan\theta_*)\cos\theta \, l_r = -J_A\ddot{\theta} \tag{8}$$

In dimensionless form equation 8 becomes:

$$\frac{1-X^2}{4} + \tilde{k}(\sin\theta - \sin\theta_*)\left(X\frac{l}{h_d}\right)^2 = -\frac{J_A\ddot{\theta}}{\rho g h_u^2 l^2} \tag{9}$$

Where $\tilde{k} = \frac{k}{\rho g \cos\theta_*}\left(\frac{l_r}{l}\right)^2$ is the total device stiffness which only depends on the geometrical configuration of the stiffener device. This equation will be solved by a 4th order Runge-Kutta method. If a quasi-steady solution is assumed, the second term becomes null and then the opening angle is directly given (hydrostatic balance) (Eq. 10). The quasi-steady assumption appears reasonable because the gate movement is slow.

$$\sin\theta = -\frac{1-X^2}{4\tilde{k}}\left(\frac{h_d}{Xl}\right)^2 + \sin\theta_* \qquad (10)$$

The design consists of choosing the distance between the sidewall and the stiffener (l_r), and the stiffener stiffness (k).

In the first step, the quasi steady assumption is evaluated on a model tide from French river Charentes mouth where several fresh marshes are present (figure 10). The water depth in the marsh (h_d) is constant and equal to 2 m. The tide amplitude is 4 m and averaged level is 1.5 m. The tide gate considered has a weight m=1000 kg, a width l=2 m and a thickness e=0.2 m. Then the inertia moment is $J_A = m/3(e^2 + l^2)$.

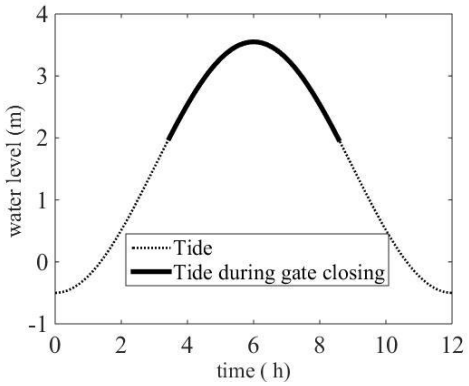

Figure 9. complete tide and during the tide gate closing for example considered.

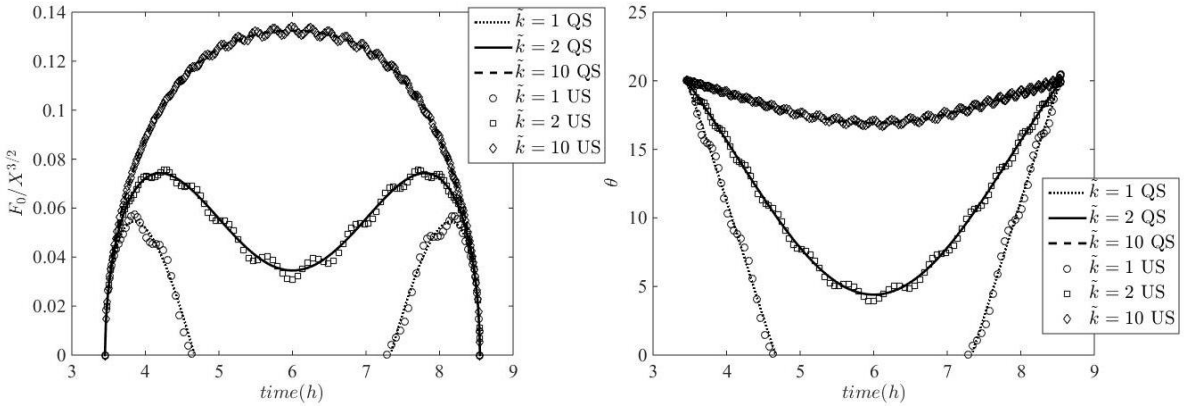

Figure 10. flowrate and opening angle for various stiffener stiffness for quasi steady calculation (QS) or unsteady calculation (US). Computation for l/h_d =1 and $\theta_* = 20°$.

The objective is to regulate the discharge for a constant downstream level (water depth in the marsh). The dimensionless flowrate with h_d constant is given by $F_0/X^{3/2}$ which corresponds to the Froude number in the downstream reach. Figure 11 shows that the quasi-steady calculations provide similar results than complete unsteady resolutions of equation 9. For unsteady calculation (US), some oscillations appear for the flowrate but the opening angle is less sensitive to them. In practice, this phenomenon is not likely to exist because of mechanical and hydrodynamical friction on the gate. Figure 11 also illustrates that the stiffness can have an influence on discharge for value between 1 and 10 for l/h_d =1. Otherwise the gate is totally closed during a too long period or remains at a constant opening. As it has been observed (Lamarque et al. 2012) that the glass eel flow into the marsh at the beginning of the

tide inversion, the design has to verify that for a given tide the angle opening is sufficiently large during one or two hours.

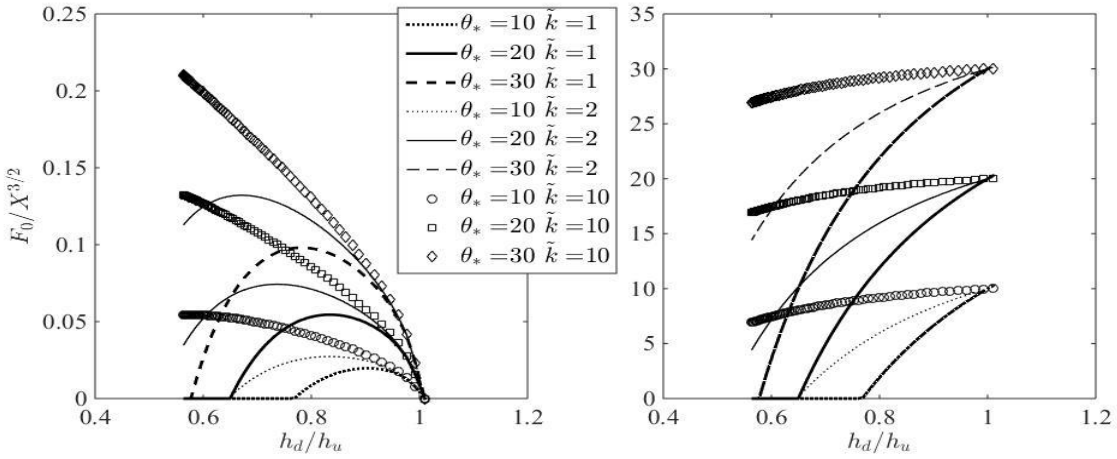

Figure 11. flowrate and opening angle for various stiffener stiffness and opening angle before contact with the gate θ* (*lr*/*l*=1, *l*/h_d =1).

The maximum discharge permitted in the marsh is selected with the opening angle θ_*. When this choice is made (θ_*=20° for example), Figures 11 and 12 show that it is possible to reduce the flowrate with the choice of the stiffener stiffness. We recall that if the stiffness *k* could not be modified, $\tilde{k}$ can be changed by choosing the appropriate length l_r. For the configuration presented here (*l*/h_d=1), the gate can be totally closed for $\tilde{k} = 1$. When the flow direction changes (h_d /h_u ~1), the opening remains sufficient to enables passability during less than 1 hour for θ_*=20°.

To emphasize the advantage of the stiffener device, the entering water volume is compared with the solution with a constant block. In Figure 13, it can be seen that the range of the stiffness is limited, for example between 1 and 2 for the considered gate. For higher values, the gate is always open and for lower values the time available for the passability is too short as deduced from previous analysis. This result proves the importance to have a design tool which ensures an efficient device. Equations 6 and 9 (with quasi steady assumption) provide a precious help to install stiffener device and adapt it to real scale tide gate. They can be simply solved when the tide (*X* as a function of time) and the gate geometry are defined.

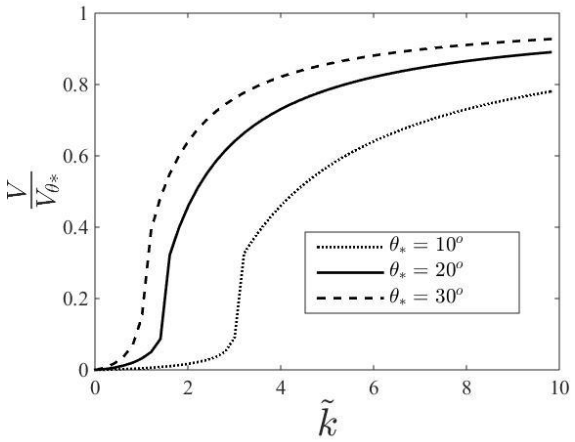

Figure 12. ratio of the saltwater intrusion volume into the marsh with stiffener (*V*) to saltwater intrusion volume with block $V_{\theta*}$.

5. Conclusion

The design of a stiffener device has been studied to allow glass eels passing a tide gate with a limitation of saltwater intrusion. In a first step, it was needed to estimate the discharge coefficient of a tide gate, which has been established by shallow water simulation, energy balance and experiments. The first 2 methods are complementary and are validated by the experiments. The variation of the discharge coefficient is then obtained and the tide gate behavior is simulated during a tide.

A global view of the movement equation suggests that quasi steady equations are pertinent and sufficient to design stiffener device. Thanks the example of a real scale tide gate, we put forward the possibility to increase passability without large impact on water intrusion. The design process was described, then the impact of the various pertinent solutions was evaluated. In the future, similar studies could be carried out considering top-hinged gate which are also very frequent. The energy momentum balance approach could be interesting to estimate C_d for larger opening for other flow control applications.

6. Acknowledgements

This work was conducted with the financial support of the Agence Française pour la Biodiversité under the grant "hydrodynamic modelling for ecohydraulics" (2017-2019).

7. References

Belaud, G., Cassan, L.and Baume, J-P (2009). Calculation of Contraction Coefficient under Sluice Gates and Application to discharge Measurement. *Journal of Hydraulic Engineering*, 135 (12). pp. 1086-1091

Boys, C. A., Kroon, F.J., Glasby, T.M., and Wilkinson, K. (2012). Improved fish and crustacean passage in tidal creeks following floodgate remediation. *Journal of Applied Ecology*, 49:223-233.

Cassan, L. and Belaud, G. (2012) . Experimental and Numerical Investigation of Flow under Sluice Gates. *Journal of Hydraulic Engineering*, 138 (4).

Lamarque M., Rigaud C., Alric A., and Baran P., 2012. Evaluation du comportement des civelles au droit d'un ouvrage à la mer et test de la modalite de gestion hivernal. *Rapport Onema/Irstea* (in French)- Programme R&D Anguilles/Ouvrage.

Lauronce, Vanessa; Bouyssonnie, William; and Rigaud, C., "Session B1: Fish-Friendly Management of First Dams in the Tidal Area of the Gironde Estuary (France, SW)" (2015). *International Conference on Engineering and Ecohydrology for Fish Passage*. 24.

Tran Dung, T., Chorda, J., Laurens, P. and Cassan, L. (2015). Modelling nature-like fishway flow around unsubmerged obstacles using a 2D shallow water model. *Environmental Fluid Mechanics.* 16 (n° 2), pp. 413-42.

Wang, R-W., David, L. and Larinier, M. (2010). Contribution of experimental fluid mechanics to the design of vertical slot fish passes. Knowledge and Management of Aquatic Ecosystems, 396.

Wright, G., Wright, R., and Kemp, P. (2014). Impact of tide gates on the migration of juvenile sea trout, salmo trutta. *Ecological Engineering*, 71:615-622.